

# Extreme beam attenuation in double-slit experiments: Quantum and subquantum scenarios

Gerhard Grössing<sup>1</sup>, Siegfried Fussy<sup>1</sup>, Johannes Mesa Pascasio<sup>1,2</sup>, and Herbert Schwabl<sup>1\*</sup>

<sup>1</sup>*Austrian Institute for Nonlinear Studies, Akademiehof,  
Friedrichstr. 10, 1010 Vienna, Austria and*

<sup>2</sup>*Atominstitut, TU Wien, Operng. 9, 1040 Vienna, Austria*

(Dated: June 16, 2021)

## Abstract

Combining high and low probability densities in *intensity hybrids*, we study some of their properties in double-slit setups. In particular, we connect to earlier results on beam attenuation techniques in neutron interferometry and study the effects of very small transmission factors, or very low counting rates, respectively, at one of the two slits. We use a “superclassical” modeling procedure which we have previously shown to produce predictions identical with those of standard quantum theory. Although in accordance with the latter, we show that there are previously unexpected new effects in intensity hybrids for transmission factors below  $a \lesssim 10^{-4}$ , which can eventually be observed with the aid of weak measurement techniques. We denote these as *quantum sweeper* effects, which are characterized by the bunching together of low counting rate particles within very narrow spatial domains. We give an explanation of this phenomenology by the circumstance that in reaching down to ever weaker channel intensities, the nonlinear nature of the probability density currents becomes ever more important, a fact which is generally not considered – although implicitly present – in standard quantum mechanics.

Keywords: quantum mechanics, neutron interferometry, double-slit experiment, beam attenuation, subquantum mechanics.

---

\* Corresponding author: [ains@chello.at](mailto:ains@chello.at)

## 1. INTRODUCTION

Continuing the search for new, and perhaps surprising, features of quantum systems, one option is to steadily decrease the intensity of a channel in one spatially constrained area, as compared to a reference intensity in another, equally constrained area. For example, one can employ the usual double-slit experiments and modify one of the two slits' channels such that the corresponding outgoing probability density is very low compared to that of the other slit. We call a combination of such distributions of high and low probability densities, or intensities, respectively, *intensity hybrids*.

Since the 1980ies, one possibility to experimentally establish and probe such hybrids has been through the introduction of beam attenuation techniques, as demonstrated in the well-known papers by Rauch's group in neutron interferometry [1, 2]. In the present paper, we re-visit these experiments and results from a new perspective, and we also discuss new, previously unexpected effects. For, our group has in recent years introduced a "superclassical" approach to describe and explain quantum behavior as an emergent phenomenon in between classical boundary conditions on the one hand, and an assumed classical subquantum domain at vastly smaller spatial scales on the other [3–11]. Here we are going to apply our approach to the above-mentioned intensity hybrids. Our main result is that in employing ever weaker channel intensities, nonlinear effects become ever more important, which are generally not considered – although implicitly present – in ordinary quantum mechanics, but which are a crucial characteristic of subquantum models as the one developed by our group. Experimental tests are feasible with the aid of weak measurement techniques.

## 2. DETERMINISTIC AND STOCHASTIC BEAM ATTENUATION IN THE DOUBLE SLIT AND THEIR SUPERCLASSICAL MODELING

### 2.1 Beam attenuation in neutron interferometry

Deterministic and stochastic beam attenuation have been studied extensively in neutron interferometry, beginning with the work by Rauch and Summhammer in 1984 [1]. More recently, an interesting model of these results has been presented by De Raedt *et al.* [12] with the aid of event-by-event simulations, thus confirming the possibility to describe the known results even without the use of quantum mechanics. Our approach, in contrast,

though also not relying on the quantum mechanical formalism, nevertheless is an attempt at a “deeper level” modeling from which the quantum mechanical results are expected to emerge. In other words, as our model is intended ultimately to go beyond standard quantum mechanics, but also to provide the quantum results as a limiting case, we shall first use the physics of beam attenuation as a means to verify the agreement with the quantum mechanical predictions. In a second step, then, we shall exploit the “extremes” of the quantum as well as of our superclassical descriptions, respectively, i.e. consider parameter values that cover a vast range of orders of magnitude so as to study extreme examples of intensity hybrids as introduced in the first Section. We shall then find results that look rather surprising from the viewpoint of standard quantum mechanics, but are fully understandable with our model.

In [1, 2], a beam chopper was used as a deterministic absorber in one arm of a two-armed interferometer, whereas for stochastic absorption semitransparent foils of various materials were used. Despite the net effect of the same percentage of neutrons being attenuated, the quantum mechanical formalism predicts the following different behaviors for the two cases. Introducing the *transmission factor*  $a$  as the beam’s transmission probability, in the case of a (deterministic) chopper wheel it is given by the temporal open-to-closed ratio,  $a = \frac{t_{open}}{t_{open}+t_{closed}}$ , whereas for a (stochastic) semitransparent material defined by its absorption cross section, it is simply the relation of the intensity  $I$  with absorption compared to the intensity  $I_0$  without, i.e.  $a = I/I_0$ . Thus the beam modulation behind the interferometer is obtained in the following two forms. For the deterministic chopper system the intensity is, with  $\varphi$  denoting the phase difference, given by

$$I \propto (1 - a) |\Psi_1|^2 + a |\Psi_1 + \Psi_2|^2 \propto 1 + a + 2a \cos \varphi, \quad (2.1)$$

whereas for stochastic beam attenuation with the semitransparent material it is

$$I \propto |\Psi_1 + \Psi_2|^2 \propto 1 + a + 2\sqrt{a} \cos \varphi. \quad (2.2)$$

In other words, although the same number of neutrons is observed in both cases, in the first one the contrast of the interference pattern is proportional to  $a$ , whereas in the second case it is proportional to  $\sqrt{a}$ .

In our accounting for the just described attenuation effects, we choose the usual double slit scenario, primarily because this will be very useful later on when discussing more extreme intensity hybrids. However, before describing the results a brief review is in order to indicate

the essentials of our model which are employed in our explanation of the beam attenuation phenomena.

## 2.2 Short review of the superclassical approach to quantum mechanics

Throughout the last years we have developed an approach to quantum mechanics within the scope of theories on “Emergent Quantum Mechanics”. (For the proceedings of the first two international conferences devoted to this subject, see [13, 14].) Essentially, we consider the quantum as a complex dynamical phenomenon, rather than as representing some ultimate-level phenomenon in terms of, e.g., pure formalism, wave mechanics, or strictly particle physics only. Our assumption is that a particle of energy  $E = \hbar\omega$  is actually an oscillator of angular frequency  $\omega$  phase-locked with the zero-point oscillations of the surrounding environment, the latter of which containing both regular undulatory and fluctuating components and being constrained by the boundary conditions of the experimental setup via the emergence of standing waves. In other words, the particle in this approach is an off-equilibrium steady-state maintained through the “sub-quantum arrow of time”, in T. Nieuwenhuizen’s [15] terminology, i.e. by the throughput of zero-point energy from its vacuum surroundings. This is in close analogy to the bouncing/walking droplets in the experiments of Couder and Fort’s group [16–18], which in many respects can serve as a classical prototype guiding our intuition. However, we denote our whole ansatz as “superclassical” [14], because it connects the classical physics at vastly different scales, i.e. the ordinary classical one and an assumed subquantum one, with “new” effects emergent on intermediate scales, which we have come to know and describe as quantum ones.

In fact, throughout the years we have succeeded in reproducing a number of quantum mechanical results with our superclassical model, i.e. without any use of the quantum mechanical formalism, like states, wave functions, *et cetera*. Note, moreover, that a Gaussian emerging from, say, a single slit with rounded edges (so as to avoid diffraction effects) is in our model the result of statistically collecting the effects of the aleatory bouncing of our particle oscillator, and thus not an ontic entity *per se*. Rather, the Gaussian stands for the statistical mean of the “excitation” (or “heating up”) of the medium within the confines of the slit, and later, as the bouncer/walker progresses, further away from it. We have described this in terms of a thermal environment that represents stored kinetic energy in the vacuum

and that is responsible for where the particle is being guided to. For example, consider particle propagation coming out from a Gaussian slit. For a particle exactly at the center of the Gaussian, the diffusive momentum contributions from the heated up environment will on average cancel each other for symmetry reasons. However, the further off the particle is from that center, the stronger the symmetry will be broken, thus resulting in a position-dependent net acceleration or deceleration, respectively – in effect, resulting in the decay of the wave packet. (For a detailed analysis, see [5].) In other words, due to wave-like diffusive propagations originating from the particle’s bounces to stir up the medium of the vacuum, particle paths can be influenced by the agitations of the vacuum even in places where no other particle is around. This will be important for the discussion of intensity hybrids later on.

The essential features of our model can be summarized as follows. As already mentioned, we have shown that the spreading of a wave packet can be exactly described by combining the forward (convective) with the orthogonal diffusive velocity fields. The latter fulfill the condition of being unbiased w.r.t. the convective velocities, i.e. the orthogonality relation for the *averaged* velocities derived in [5] is  $\overline{\mathbf{v}\mathbf{u}} = 0$ , since any fluctuations  $\mathbf{u} = \delta(\nabla S/m)$  are shifts along the surfaces of action  $S = \text{const}$ . Moreover, the fluctuations can be directed towards the left or towards the right from the mean (i.e. from the Ehrenfest trajectory), which leads us to introduce the notations  $\mathbf{u}_{iL}$  and  $\mathbf{u}_{iR}$ , respectively.

Reducing the general case discussed in [10] to the double-slit case, we note for the first and second channels the emergent velocity vectors  $\mathbf{v}_{1(2)}$ ,  $\mathbf{u}_{1(2)R}$ , and  $\mathbf{u}_{1(2)L}$  with associated amplitudes  $R_{1(2)}$ , respectively. In order to completely accommodate the totality of the system of currents present, we obtain a local wave intensity for any velocity component, e.g. for  $\mathbf{v}_1$ , by the pairwise projection on the unit vector  $\hat{\mathbf{v}}_1$  weighted by  $R_1$  of the totality of all amplitude weighted unit velocity vectors being operative at  $(\mathbf{x}, t)$ :

$$P(\mathbf{v}_1) = R_1 \hat{\mathbf{v}}_1 \cdot (\hat{\mathbf{v}}_1 R_1 + \hat{\mathbf{u}}_{1R} R_1 + \hat{\mathbf{u}}_{1L} R_1 + \hat{\mathbf{v}}_2 R_2 + \hat{\mathbf{u}}_{2R} R_2 + \hat{\mathbf{u}}_{2L} R_2). \quad (2.3)$$

Due to the mentioned orthogonality between  $\mathbf{v}_i$  and  $\mathbf{u}_{iL(R)}$ , i.e. with  $\hat{\mathbf{v}}_1 \cdot \hat{\mathbf{v}}_2 =: \cos \varphi$ , but  $\hat{\mathbf{v}}_i \cdot \hat{\mathbf{u}}_{iL(R)} = 0$  *et cetera*, and with the trivial relation  $\hat{\mathbf{u}}_{iR} R_i + \hat{\mathbf{u}}_{iL} R_i = 0$ ,  $i = 1, 2$ , we finally

obtain

$$P(\mathbf{v}_1) = R_1^2 + R_1 R_2 \cos \varphi \quad (2.4)$$

$$P(\mathbf{u}_{1R}) = -P(\mathbf{u}_{1L}) = \sin \varphi \quad (2.5)$$

$$P(\mathbf{v}_2) = R_2^2 + R_1 R_2 \cos \varphi \quad (2.6)$$

$$P(\mathbf{u}_{2R}) = -P(\mathbf{u}_{2L}) = -\sin \varphi \quad (2.7)$$

leading to the probability densities  $P_i$  for each channel,  $i = 1$  or  $2$ ,

$$P_1 = R_1^2 + R_1 R_2 \cos \varphi \quad (2.8)$$

$$P_2 = R_2^2 + R_1 R_2 \cos \varphi. \quad (2.9)$$

The total probability density  $P_{\text{tot}}$  for the double-slit case is then simply given by  $P_{\text{tot}} = P_1 + P_2$ . The local current attributed to each velocity component is defined as the corresponding “local” intensity-weighted velocity, e.g. for  $\mathbf{v}_1$  it is given as  $\mathbf{J}(\mathbf{v}_1) = \mathbf{v}_1 P(\mathbf{v}_1) = \mathbf{v}_1 (R_1^2 + R_1 R_2 \cos \varphi)$ . The local intensity of a partial current is dependent on all other currents, and the total current itself is composed of all partial components, thus constituting a representation of what we call *relational causality*. The total current consequently reads as  $\mathbf{J}_{\text{tot}} = \mathbf{v}_1 P(\mathbf{v}_1) + \mathbf{u}_{1R} P(\mathbf{u}_{1R}) + \mathbf{u}_{1L} P(\mathbf{u}_{1L}) + \mathbf{v}_2 P(\mathbf{v}_2) + \mathbf{u}_{2R} P(\mathbf{u}_{2R}) + \mathbf{u}_{2L} P(\mathbf{u}_{2L})$ , which, by identifying the resulting diffusive velocities  $\mathbf{u}_{iR} - \mathbf{u}_{iL}$  with the effective diffusive velocities  $\mathbf{u}_i$  for each channel, finally leads to

$$\mathbf{J}_{\text{tot}} = R_1^2 \mathbf{v}_1 + R_2^2 \mathbf{v}_2 + R_1 R_2 (\mathbf{v}_1 + \mathbf{v}_2) \cos \varphi + R_1 R_2 (\mathbf{u}_1 - \mathbf{u}_2) \sin \varphi. \quad (2.10)$$

The trajectories or streamlines, respectively, are given by

$$\dot{\mathbf{x}} = \mathbf{v}_{\text{tot}} = \frac{\mathbf{J}_{\text{tot}}}{P_{\text{tot}}}. \quad (2.11)$$

As first shown in [8], by re-inserting the expressions for convective and diffusive velocities, respectively, i.e.

$$\mathbf{v}_i = \frac{\nabla S_i}{m}, \quad \text{and} \quad \mathbf{u}_i = -\frac{\hbar}{m} \frac{\nabla R_i}{R_i}, \quad (2.12)$$

one immediately identifies Eq. (2.11) with the Bohmian guidance equation and Eq. (2.10) with the quantum mechanical pendant for the probability density current [19]. As we have shown also the latter identity, we are assured that our results are the same as those of standard quantum mechanics – provided, of course, that generally (i.e. in the standard

quantum as well as in our ansatz) the idealization of using Gaussians or similar regular distribution functions is applicable for the high degrees of attenuation studied here. However, as in our model we can also make use of the velocity field to plot the averaged particle trajectories, we can in principle provide a more detailed picture, in similar ways to the Bohmian one, but still not relying on any quantum mechanical tool like a wave function, for example.

### 2.3 Application to deterministic and stochastic beam attenuation experiments

Let us now display some typical results from our superclassical approach to beam attenuations. We can classically simulate the propagation of a Gaussian whose variance increases due to the diffusion process we implement [5]. The results are in perfect agreement with the quantum mechanical ones. This can be seen already from the resulting formulas for probability density distributions, which, despite a different approach, lead to the same final forms.

To begin, consider deterministic attenuation first. This case is also very straightforward to understand in our approach, as it just amounts to the addition of two context-dependent probability distributions, the first context being a single-slit experiment, and the second context a double-slit one. For the calculation, we just have to use the fact that in our model the intensity according to Eqs. (2.8) and (2.9) is given by the projection rule  $P_i = R_i^2 + R_i R_j \cos \varphi$  for the real-valued wave amplitudes  $R_i$  per slit  $i$  with  $j$  denoting the second slit. Keeping in mind that in the one-slit case as temporarily realized in the deterministic beam chopper experiment, the density of the single open slit is simply given as  $P'_1 = R_1^2$  [10], we have in complete agreement with (2.1) that

$$I \propto (1 - a) P'_1 + a (P_1 + P_2) \propto 1 + a + 2a \cos \varphi. \quad (2.13)$$

On the other hand, for stochastic attenuation we obtain with  $a = I/I_0$ , and thus with the amplitude of the attenuated slit (e.g. number 2) becoming  $R_2 \rightarrow \sqrt{a} R_2$ , that

$$I \propto (P_1 + P_2) \propto 1 + a + 2\sqrt{a} \cos \varphi, \quad (2.14)$$

which is in complete agreement with (2.2). In Figs. 2.1a–2.1c we show the results of our computer simulations following [5] for the probability density distributions of a neutron beam

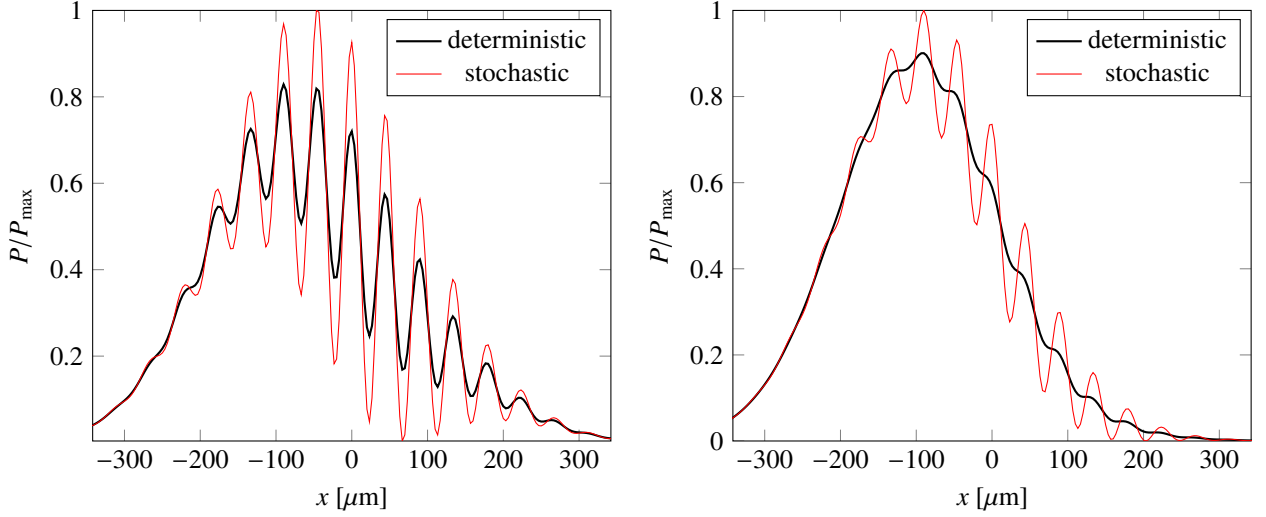
for three different values of the beam transmission factor  $a$ . The typical wavelength used is  $\lambda = 1.8 \text{ nm}$  (c.f. [20]). The Gaussian slits each are  $22 \mu\text{m}$  wide, with their centers being  $200 \mu\text{m}$  apart, and the intensity distributions are recorded on a screen located in the forward direction at a distance of 5 m from the double slit. Corresponding to the different behaviors of the contrast in deterministic and stochastic attenuation, respectively, one can see the different contributions to the overall probability density distribution, with the differences becoming smaller and smaller with ever decreasing transmission factor  $a$ . For consistency, we have also checked and confirmed that the total areas below the two curves are identical, as they must be in order to represent the same overall throughput of the number of neutrons.

In interpreting their results of the beam attenuation experiments with neutrons, the authors accordingly found evidence in support of the complementarity principle. That is, the more pronounced the visibility of the interference fringes, the less which-path knowledge one can have of the particle propagation, and *vice versa*: the higher the probability is for a particle to take a path through one certain slit, the less visible the interference pattern becomes. This was in fact confirmed in the above-mentioned neutron interferometry experiments, albeit to a lesser degree for very low counting rates. In particular, the authors of [1, 2] often use expressions such as the “particle-like” or the “wave-like” nature of the quantum system studied, depending on whether which-path information or interference effects are dominant, respectively. While this is all correct as far as the mentioned papers are concerned, an extrapolation of the use of “particle-like” or “wave-like” attributed to more extreme intensity hybrids is not guaranteed. In fact, we shall show in the following Section a particular effect which undermines said dichotomy of “particle-like” and “wave-like” features, thereby calling for an improved, more general analysis of possible relationships between particle and wave features.

### 3. PHENOMENOLOGY OF THE QUANTUM SWEEPER FOR COHERENT AND INCOHERENT BEAMS

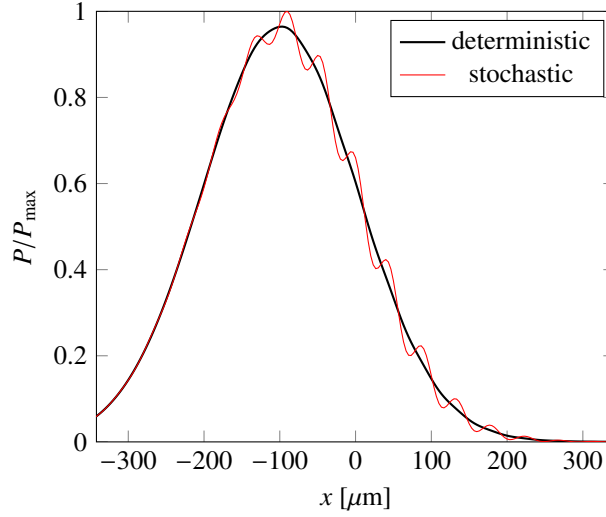
We assume a coherent beam in a double-slit experiment, with the intensity distribution being recorded on a screen, and we are going to discuss a particular effect of the stochastic attenuation of one of the two emerging Gaussians at very small transmission factors. With the appropriate filtering of the particles going through one of the two slits, the recorded





(a)  $a = 0.25$ .

(b)  $a = 0.025$ .



(c)  $a = 0.0025$ .

Figure 2.1: Superclassical simulation of probability density distributions with beam attenuation  $a$  at slit 2.

probability density on a screen in the surroundings of the experiment will appear differently than what one would normally expect. That is, even if one had a low beam intensity coming from one slit, one would expect the following scenario according to the usual quantum mechanical heuristics: The interference pattern would more and more become asymmetric in the sense that the contributions from the fully open slit would become dominant until such a low counting rate from the attenuated slit is arrived at that essentially one would

have a one-slit distribution of recorded particles on the screen. This tendency is at least clearly visible in Figs. 2.1a–2.1c, and one would only expect for ever smaller values of  $a$  that the oscillatory behavior of the stochastic case would more and more disappear to finally merge with the smoothed-out pattern of an essentially one-slit distribution pattern.

Interestingly, this is not exactly what one obtains at least for very low values of  $a$  when going through the calculations and/or computer simulations with our superclassical bouncer model. The latter consists, among other features, in an explicit form of the velocity field emerging from the double slit, as well as of the probability density current associated with it.

Fig. 3.1 shows the “quantum sweeper” effect: a series of probability density distributions plus averaged trajectories for the case that the intensity in slit 2 is gradually diminished. We use the same model as in [8], or [21], respectively: particles (represented by plane waves in the forward  $y$ -direction) from a coherent source passing through “soft-edged” slits in a barrier (located along the  $x$ -axis) and recorded at a screen in the forward direction, i.e. parallel to the barrier. This situation is described by two Gaussians representing the totality of the effectively “heated-up” path excitation field, one for slit 1 and one for slit 2, whose centers have the same distances from the plane spanned by the source and the center of the barrier along the  $y$ -axis, respectively. Now, with ever lower values of the transmission factor  $a$  during beam attenuation, one can see a steadily growing tendency for the low counting rate particles of the attenuated beam to become swept aside. In our model, this is straightforward to understand, because we have the analytical tools to differentiate between the forward propagations  $\mathbf{v}_i$  and the diffusive influences of velocities  $\mathbf{u}_i$ , as distinguishable contributions from the different slits  $i$ . Thus, it is processes of diffusion which are seen in operation here, due to the presence of accumulated heat (i.e. kinetic energy), primarily in the “strong” beam, as discussed in the previous Section. So, in effect, we understand Fig. 3.1 as the result of the vacuum heat sweeping aside the very low intensity beam, with a “no crossing” line defined by the balancing out of the diffusive momenta,  $m(\mathbf{u}_1 + \mathbf{u}_2) = 0$ .

Importantly, for certain slit configurations and sizes of the transmission factor, the sweeper effect leads to a bunching of trajectories which may become deflected into a direction almost orthogonal to the original forward direction. In other words, one would need much wider screens in the forward direction to register them, albeit then weakened due to a long traveling distance. On the other hand, if one installed a screen orthogonal to the

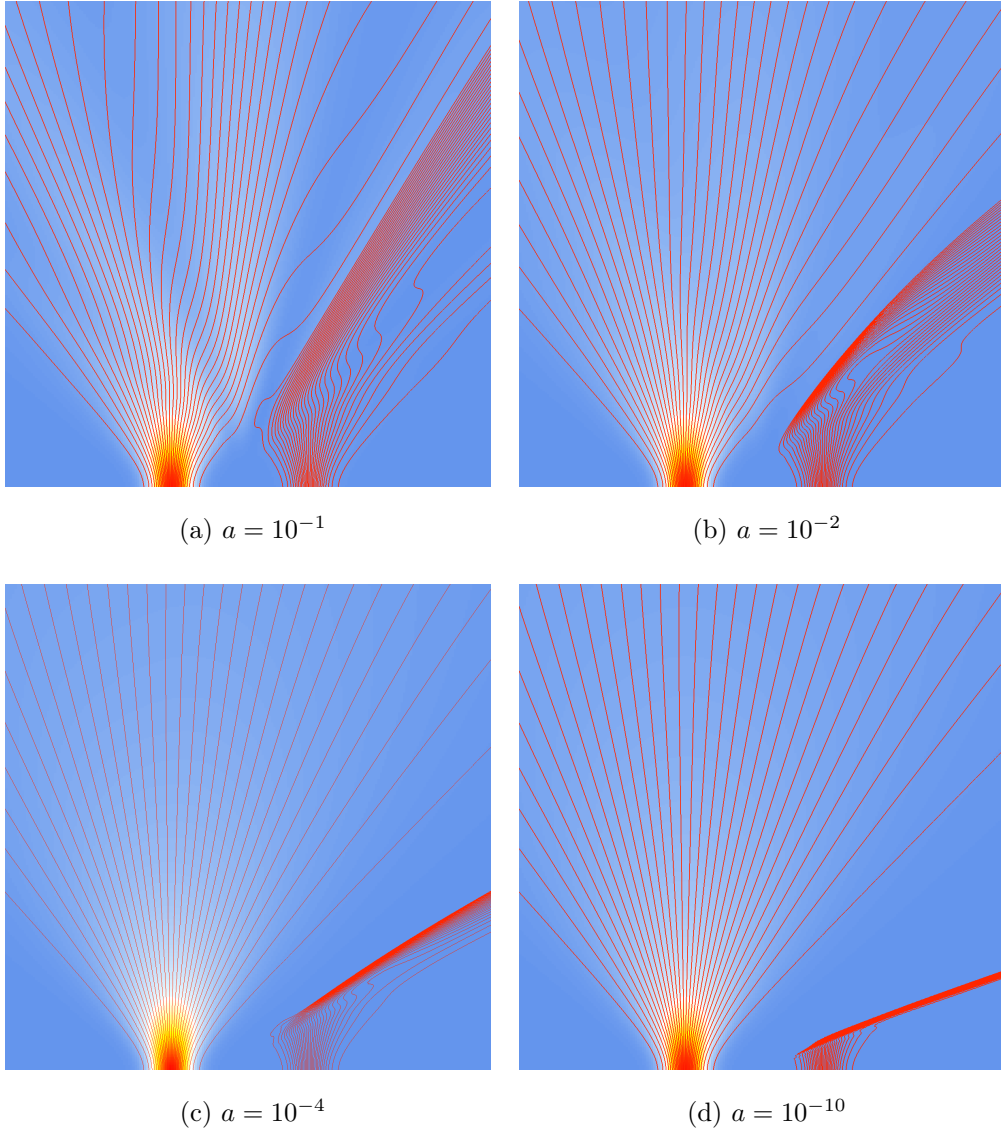


Figure 3.1: The “quantum sweeper” effect for different transmission factors  $a$ : With ever lower values of  $a$ , one can see a steadily growing tendency for the low counting rate particles of the attenuated beam to become swept aside. In our model, this phenomenology is explained by processes of diffusion, due to the presence of accumulated vacuum heat (i.e. kinetic energy) mainly in the “strong” beam. The sweeper effect is thus the result of the vacuum heat sweeping aside the very low intensity beam, with a “no crossing” line defined by the balancing out of the osmotic momenta coming from the two beams, respectively. Throughout this paper, to demonstrate the effect more clearly, we use the same number of trajectories for each slit.

“forward screen”, i.e. one that is parallel to the original forward motion (and thus to the  $y$ -axis), one could significantly improve the contrast and thus register the effect more clearly (see also Fig. 3.3 further below). Further, we note that changing the distance between the two slits does not alter the effect, but demonstrates the bunching of the low counting rate arrivals in essentially the same narrow spatial area even more drastically. So, again, if one places a screen not in the forward direction parallel to the barrier containing the double slit, but orthogonally to the latter, one registers an increased local density of particle arrivals in a narrow spatial area under an angle that is independent of the slit distance.

Let us now turn to the case of decoherent beams. For, although we shall refrain from constructing a concrete model of decoherence and implementing it in our scheme, we already have the tools of an effective theory, i.e. to describe decoherence without the need of a specified mechanism for it. Namely, as full decoherence between two (Gaussian or other) beams is characterized by the complete absence of the interference term in the overall probability distribution of the system, this means that  $P_{\text{tot}} = R_1^2 + R_2^2$ , since the interference term

$$R_1 R_2 (\mathbf{v}_1 + \mathbf{v}_2) \cos \varphi = 0. \quad (3.1)$$

If we therefore choose that on average one has  $\cos \varphi = 0$ , a situation with  $\varphi = \frac{\pi}{2}$  effectively describes two incoherent beams in the double-slit system. What about the two interference terms in the probability density current (2.10), then? Well, the first term is identical with the vanishing (3.1), but the second term, with  $\mathbf{u}_i = -\frac{\hbar}{m} \frac{\nabla R_i}{R_i}$  and  $\varphi = \frac{\pi}{2}$  explicitly reads as

$$\frac{\hbar}{m} R_1 R_2 \left( \frac{\nabla R_2}{R_2} - \frac{\nabla R_1}{R_1} \right) = \frac{\hbar}{m} (R_1 \nabla R_2 - R_2 \nabla R_1). \quad (3.2)$$

As the distributions  $R_i$  may have long wiggly tails – summing up, after many identical runs, to a Gaussian with no cutoff, but spreading throughout the whole domain of the experimental setup [9] –, the expression (3.2) is not at all guaranteed to vanish. In fact, a look at Fig. 3.2 shows that there is an effect even for incoherent beams: Although the product  $R_1 R_2$  is negligible and therefore leads to no interference fringes on the screen, nevertheless expression (3.2) has the effect of “bending” average trajectories so as to obey the “no crossing” rule well known from our model as well as from Bohmian theory.

As was already pointed out in [22], or more recently, in [23], the resulting trajectories of Fig. 3.2a can be understood as a nonlinear effect that is not usually considered in standard quantum mechanics, but explainable in the Bohmian picture. There, it is the structure of the

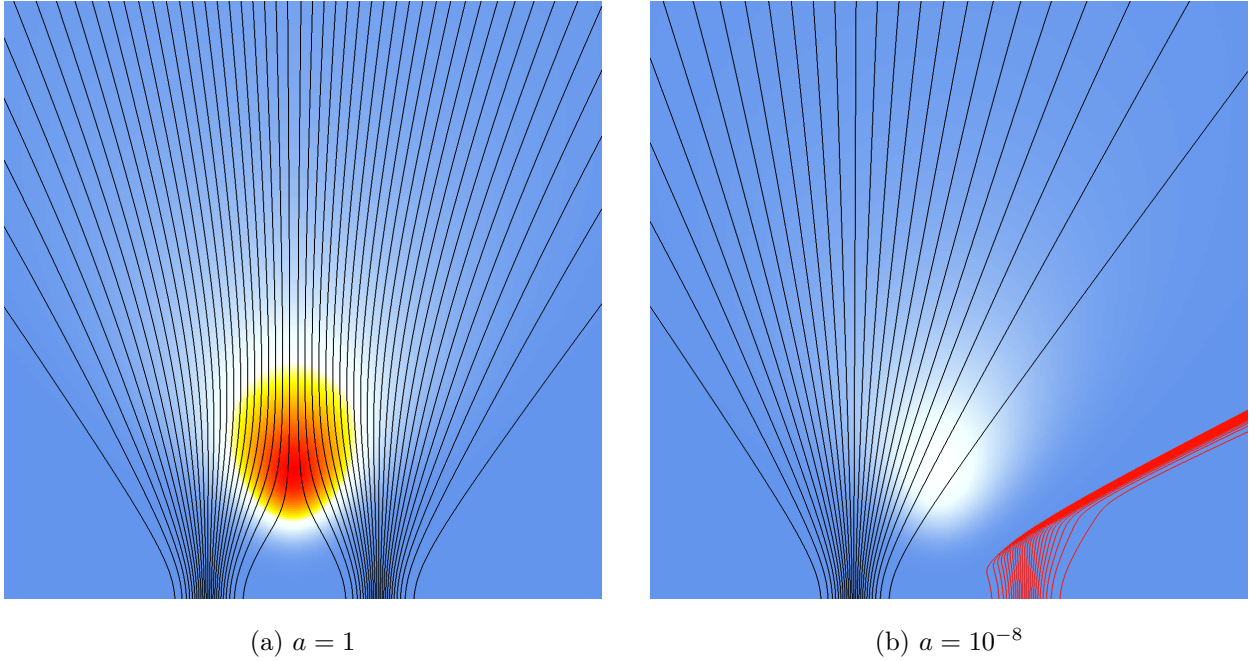


Figure 3.2: Double-slit experiment with completely incoherent channels. (a) The average trajectories never cross the central symmetry line, a fact due to the diffusion related “hot spot” indicated in red-to-yellow-to-white (depicting both interference terms of  $J_x$ ), which represents a kinetic energy reservoir that effectively gives particles a push in the forward direction. (b) The intensity of  $J_x$  is now weakened by the factor  $a = 10^{-8}$ , which is why it does not affect the “strong” beam. However, it is sufficient for the attenuated beam to become deflected.

velocity field which is genuinely nonlinear and therefore allows for the emergence of the type of trajectory behavior which has in earlier years sometimes even been labeled as “surreal”. However, also in our approach, the emergence of the trajectories of Fig. 3.2 is completely understandable as it can be traced back to the non-vanishing of expression (3.2). Whereas in a naive extrapolation of what one is used to in standard quantum mechanics, the currents per channel would – just like the probability distributions  $R_i^2$  themselves – go down linearly with ever lowered intensity, this is actually not the case: It is the nonlinear behavior of the amplitudes and their gradients, respectively, that are the cause of the observed trajectory behavior in our simulations.

In sum, then, performing a double-slit experiment with decoherent beams leads to an emergent behavior of particle propagation which can be explained by the effectiveness of

diffusion waves with velocities  $u_i$  interacting with each other, thereby creating a “hot spot” where the intensity of the diffusive currents is highest and leads to a deflection into the forward direction such that no crossing of the average velocities beyond the symmetry line is made possible (Fig. 3.2a). This is therefore in clear contradiction to the scenario where only one slit is open for the particle to go through. If the slits are not open simultaneously, the particles could propagate to locations beyond the symmetry line, i.e. to locations forbidden in the case of the second slit being open. [22]

As our velocity fields  $\mathbf{v}_i$  and  $\mathbf{u}_i$ , Eq. (2.12), are identical with the Bohmian and the “osmotic” momentum, respectively, one can relate them also to the technique of weak measurements. The latter have turned out [24–26] to provide said velocities as “weak values”, which are just given by the real and complex parts of the quantum mechanical expression  $\frac{\langle \mathbf{r} | \hat{p} | \Psi(t) \rangle}{\langle \mathbf{r} | \Psi(t) \rangle}$ , i.e. the weak values associated with a weak measurement of the momentum operator  $\hat{p}$  followed by the usual (“strong”) measurement of the position operator  $\hat{r}$  whose outcome is  $\mathbf{r}$ . In other words, in principle the trajectories for intensity hybrids generally, and for the quantum sweeper in particular, are therefore accessible to experimental confirmation.

Finally, let us stress the relevance of our finding w.r.t. the issue of wave-particle duality. Considering the appearance of compressed interference fringes in the attenuated beam in Fig. 3.1, it is indisputable that one has to do with the result of a wave-like behavior. This is confirmed in Fig. 3.2b where the decoherent scenario is characterized by the complete absence of such wave-like behavior like interference fringes. This means, however, that an often used argument to describe the complementarity between wave- and particle-like behavior in the double slit experiment, or in interferometry, respectively, has only limited applicability, as it does not apply to intensity hybrids, since in our model the wave-like contributions due to diffusion are always present. Specifically, the relation for pure states [27]

$$D^2 + V^2 = 1, \quad (3.3)$$

with distinguishability  $D = \left| \frac{R_1^2 - R_2^2}{R_1^2 + R_2^2} \right|$  representing the particle-related which-path information and visibility  $V = \frac{|R_1 + R_2|^2 - |R_1 - R_2|^2}{|R_1 + R_2|^2 + |R_1 - R_2|^2} = \frac{2R_1 R_2}{R_1^2 + R_2^2}$  the contrast of the interference fringes in the standard quantum mechanical double slit scenario suggests that with ever lower values of  $a$  ever lower values of  $V$  are implied in a constantly decreasing manner. In our case, by considering the superclassical nature of the sweeper effect, we find a deviating, characteristic signature at very low values of  $a \lesssim 10^{-4}$ . In this domain, the usual expectation would be

that practically one has arrived at the “particle” side of the complementarity principle, i.e. essentially a one-slit distribution, with wave-like phenomena having almost disappeared. However, if one has a very strongly attenuated beam, the emerging behavior of its outgoing trajectories is different from a one-slit particle distribution scenario if the other slit is open and un-attenuated. In this case, the wave-like phenomena do appear, but are restricted solely to the attenuated beam (Fig. 3.3), a fact that we attribute to the appearance of nonlinear effects of the probability density current (2.10). As already mentioned, the increased local relative contrast corresponding to a bunching of trajectories and due to said nonlinear effect of the probability density current is to be captured by a vertical screen (i.e. parallel to the  $y$ -axis) for optimal visibility.

In the standard quantum mechanical description of double-slit experiments with intensity hybrids one is usually only concerned with the gradual fading out of wave-like properties like interference fringes. However, in our superclassical model we are dealing with diffusion-based wave-like properties throughout all magnitudes of attenuation of e.g., slit 2, even in the case of incoherent beams. For here, if we observe particles coming through slit 2 characterized by a very low intensity such as  $a = 10^{-8}$ , one faces the sweeper effect. (Fig. 3.3)

The number  $n(a)$  of particles which we do see come through slit 2 and which produces the distribution (red) in Fig. 3.3a actually is deflected from the “forward” screen when slit 1 is opened, but the same number  $n(a)$  can easily be detected on the sideways screen to the right in Fig. 3.3b. Although the particles would eventually also be detected on a more elongated forward screen, the effect would be much smaller simply due to the geometry, whereas the sideways screen setup allows the registration with maximal contrast. In principle, for beam attenuations as schematized in Fig. 3.3, if one employs a sideways screen, one thus obtains a different outcome than the one expected due to standard quantum mechanical lore. According to the latter, the beam from slit 2 should be unaffected by the situation at slit 1. This would mean that in the unaffected scenario less than a number of  $\frac{n(a)}{2}$  particles could eventually be registered on any sideways screen parallel to the  $y$ -axis along a wide spatial extension, whereas our result predicts that the totality of the number  $n(a)$  of particles can be registered within a comparatively narrow spatial domain. In Fig. 3.3c, the vertical screen setup reveals interesting features of the probability density distribution, accounting both for the interference and the sweeper effects. The black line indicates the continuation of the probability density distribution for the one-slit case, which is of course

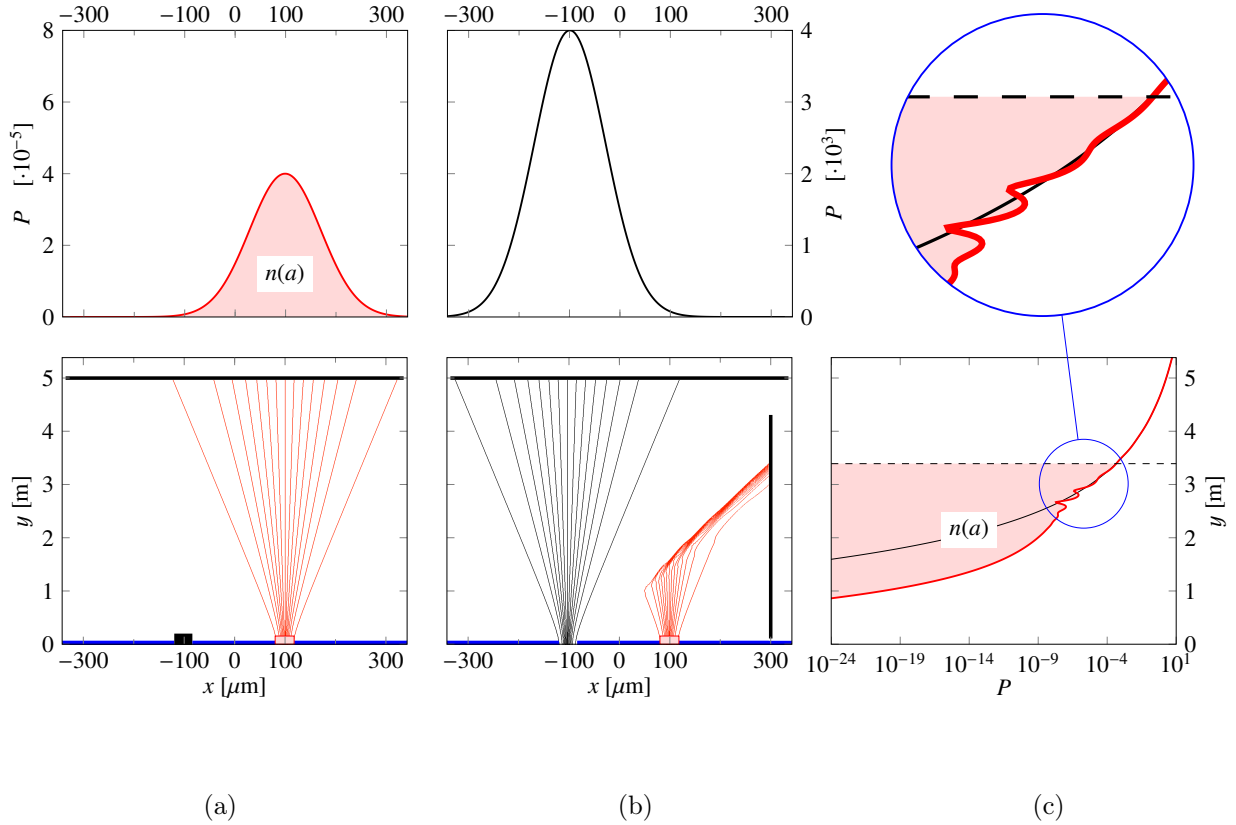


Figure 3.3: Registration of particles during extreme beam attenuation,  $a = 10^{-8}$ . (a) If slit 1 is closed, a small number  $n(a)$  of particles coming from slit 2 is registered on the forward screen. (b) If, then, slit 1 is fully opened (i.e. with  $a = 1$ ), one registers a much higher number of particles for slit 1, but apparently none for slit 2. Instead,  $n(a)$  particles are then registered on the sideways screen parallel to the  $y$ -axis. (c) The probability density distribution for the latter exhibits marked signs of interference effects due to the compressed wave superpositions within the bunching area caused by the sweeper effect.

being modified once the interference effect in the coherent case of adding an attenuated beam is allowed for. However, even in the incoherent scenario not showing the comparatively small interference effects, one still obtains the full sweeper effect, with a smooth transition between the two curves in the upper and the lower parts of Fig. 3.3c, respectively. This is due to the non-vanishing of (3.2), i.e. a significant contribution from the diffusive terms despite the smallness of the transmission factor  $a$ .



## 4. SUMMARY

Summarizing, we have shown that for transmission factors below  $a \lesssim 10^{-4}$  in intensity hybrids, new effects appear which are not taken into account in a naive, i.e. linear, extrapolation of expectations based on higher-valued transmission factors. We have described the phenomenology of these “quantum sweeper” effects, including the bunching together of low counting rate particles within a very narrow spatial domain, or channel, respectively. However, we also stress that these results are in accordance with standard quantum mechanics, since we just used a re-labeling and re-drawing of the constituent parts of the usual quantum mechanical probability density currents. The reason why the above-mentioned naive expectations are not met is given by the explicit appearance of the nonlinear structure of the probability density current in these domains for very low values of  $a$ . In this regard, our subquantum model is better equipped to deal with these appearances explicitly.

## ACKNOWLEDGMENTS

We thank the Fetzer Franklin Fund for partial support of the current work.

- 
- [1] H. Rauch and J. Summhammer, “Static versus time-dependent absorption in neutron interferometry,” *Phys. Lett. A* **104** (1984) 44–46.
  - [2] H. Rauch, J. Summhammer, M. Zawisky, and E. Jericha, “Low-contrast and low-counting-rate measurements in neutron interferometry,” *Phys. Rev. A* **42** (1990) 3726–3732.
  - [3] G. Grössing, “The vacuum fluctuation theorem: Exact Schrödinger equation via nonequilibrium thermodynamics,” *Phys. Lett. A* **372** (2008) 4556–4563, [arXiv:0711.4954 \[quant-ph\]](#).
  - [4] G. Grössing, “On the thermodynamic origin of the quantum potential,” *Physica A* **388** (2009) 811–823, [arXiv:0808.3539 \[quant-ph\]](#).
  - [5] G. Grössing, S. Fussy, J. Mesa Pascasio, and H. Schwabl, “Emergence and collapse of quantum mechanical superposition: Orthogonality of reversible dynamics and irreversible diffusion,” *Physica A* **389** (2010) 4473–4484, [arXiv:1004.4596 \[quant-ph\]](#).

- [6] G. Grössing, S. Fussy, J. Mesa Pascasio, and H. Schwabl, “Elements of sub-quantum thermodynamics: Quantum motion as ballistic diffusion,” *J. Phys.: Conf. Ser.* **306** (2011) 012046, [arXiv:1005.1058 \[physics.gen-ph\]](#).
- [7] G. Grössing, J. Mesa Pascasio, and H. Schwabl, “A classical explanation of quantization,” *Found. Phys.* **41** (2011) 1437–1453, [arXiv:0812.3561 \[quant-ph\]](#).
- [8] G. Grössing, S. Fussy, J. Mesa Pascasio, and H. Schwabl, “An explanation of interference effects in the double slit experiment: Classical trajectories plus ballistic diffusion caused by zero-point fluctuations,” *Ann. Phys.* **327** (2012) 421–437, [arXiv:1106.5994 \[quant-ph\]](#).
- [9] G. Grössing, S. Fussy, J. Mesa Pascasio, and H. Schwabl, “‘Systemic nonlocality’ from changing constraints on sub-quantum kinematics,” *J. Phys.: Conf. Ser.* **442** (2013) 012012, [arXiv:1303.2867 \[quant-ph\]](#).
- [10] S. Fussy, J. Mesa Pascasio, H. Schwabl, and G. Grössing, “Born’s rule as signature of a superclassical current algebra,” *Ann. Phys.* **343** (2014) 200–214, [arXiv:1308.5924 \[quant-ph\]](#).
- [11] G. Grössing, S. Fussy, J. Mesa Pascasio, and H. Schwabl, “Relational causality and classical probability: Grounding quantum phenomenology in a superclassical theory,” *J. Phys.: Conf. Ser.* **504** (2014) 012006, [arXiv:1403.3295 \[quant-ph\]](#).
- [12] H. De Raedt, F. Jin, and K. Michielsen, “Discrete-event simulation of neutron interferometry experiments,” *AIP Conf. Proc.* **1508** (2012) 172–186.
- [13] G. Grössing, ed., *Emergent Quantum Mechanics 2011*. No. 361/1. IOP Publishing, Bristol, 2012. Url: <http://iopscience.iop.org/1742-6596/361/1>.
- [14] G. Grössing, H.-T. Elze, J. Mesa Pascasio, and J. Walleczek, eds., *Emergent Quantum Mechanics 2013*. No. 504/1. IOP Publishing, Bristol, 2014. Url: <http://iopscience.iop.org/1742-6596/504/1>.
- [15] T. M. Nieuwenhuizen, “A subquantum arrow of time,” *J. Phys.: Conf. Ser.* **504** (2014) 012008.
- [16] E. Fort, A. Eddi, A. Boudaoud, J. Moukhtar, and Y. Couder, “Path-memory induced quantization of classical orbits,” *PNAS* **107** (2010) 17515–17520.
- [17] Y. Couder and E. Fort, “Single-particle diffraction and interference at a macroscopic scale,” *Phys. Rev. Lett.* **97** (2006) 154101.

- [18] Y. Couder and E. Fort, “Probabilities and trajectories in a classical wave-particle duality,” *J. Phys.: Conf. Ser.* **361** (2012) 012001.
- [19] Á. S. Sanz and S. Miret-Artés, “A trajectory-based understanding of quantum interference,” *J. Phys. A: Math. Gen.* **41** (2008) 435303, [arXiv:0806.2105 \[quant-ph\]](#).
- [20] H. Rauch and S. A. Werner, *Neutron interferometry: lessons in experimental quantum mechanics*. Clarendon Press, New York, 2000.
- [21] P. R. Holland, *The Quantum Theory of Motion*. Cambridge University Press, Cambridge, 1993.
- [22] Á. S. Sanz and F. Borondo, “Contextuality, decoherence and quantum trajectories,” *Chem. Phys. Lett.* **478** (2009) 301–306, [arXiv:0803.2581 \[quant-ph\]](#).
- [23] A. Luis and A. S. Sanz, “Detection of Bohmian trajectories for mixed states,” *pre-print* (2014) , [arXiv:1311.2612 \[quant-ph\]](#).
- [24] C. R. Leavens, “Weak measurements from the point of view of Bohmian mechanics,” *Found. Phys.* **35** (2005) 469–491.
- [25] H. M. Wiseman, “Grounding Bohmian mechanics in weak values and bayesianism,” *New J. Phys.* **9** (2007) 165–165, [arXiv:0706.2522 \[quant-ph\]](#).
- [26] B. J. Hiley, “Weak values: Approach through the Clifford and Moyal algebras,” *J. Phys.: Conf. Ser.* **361** (2012) 012014, [arXiv:1111.6536v1 \[quant-ph\]](#).
- [27] D. M. Greenberger and A. Yasin, “Simultaneous wave and particle knowledge in a neutron interferometer,” *Phys. Lett. A* **128** (1988) 391–394.